CH_4 + H_2 Flames Anchored on Perforated Plates - A Thermoacoustic Analysis

Pedro Miguel Que Ye
pedro.ye@tecnico.ulisboa.pt

Instituto Superior Técnico, Universidade de Lisboa, Portugal

December 2021

Abstract

Continuous combustion applications are prone to thermoacoustic instabilities. In many of these applications, multiperforated plates (MPP) are used as flame stabilizers. Additionally, with recent climate change effects, hydrogen has been promoted as a fuel for combustion systems. Considering this, the present work focuses on the effects of MPP with different perforation ratios (ψ) and fuel blends on thermoacoustic instabilities. Experiments are done in a burner with variable length cavity (L) and MPPs with different ψ. The fuels used are 100% C_3H_8, 100% CH_4 and 90% CH_4 + 10% H_2 in volume. Evaluation of the sound pressure level (SPL), frequency and flame shape is done for the last two blends. Also, a mathematical model to predict thermoacoustic instabilities is presented. H_2 enrichment leads to more thermoacoustic instabilities and higher frequencies. With the decrease in ψ from the MPPs, these instabilities are reduced but at the cost of richer lean-blowout (LBO) limits. Flame shape analysis demonstrates that higher frequencies are associated with a shortening of the unstable length of the flame. The mathematical model predicts more instabilities with the addition of H_2 and higher ψ. However, its results are deviated from the experiments.
Keywords: Thermoacoustic Instabilities, Perforated Plates, Hydrogen, Methane, Perforation Ratio

1. Introduction

Systems with continuous combustion application can have different operation modes, but they are limited by thermoacoustic instabilities which are often expressed in the form of noise and low intensity vibration. In some cases the oscillations can reduce the components life time or lead to complete failure of the system.

If there is unsteady combustion and acoustic waves propagating in the system, the coupling between them can lead to thermoacoustic combustion instabilities. These happen when resonance, *i.e.* oscillations at frequencies with the highest amplification factor, occurs. When there is a pressure wave emitted by the surroundings or by the flame heat release, the oscillation might be amplified by the cavity, generating a perturbation in the feeding flow. Consequently if the perturbation is in phase with the flame it will enhance its oscillation creating a feedback loop and therefore, developing self-sustained instabilities.

The criterion which leads to combustion instabilities and consequently to the sound generation was first documented by Rayleigh [1] and described that for resonance to be encouraged, the system needs to be fed energy when the working fluid is expanding and removed energy when it is compressing, doubling down on the effects of expansion and compression, which consequently enhances the oscillation's amplitude. A mathematical representation of the Rayleigh criterion was first introduced by Putnam and Dennis [2]. However, the formulation did not take into account the acoustic losses through viscous dissipation and dependency on time and space. Considering this, Zinn [3] formulated a more appropriate equation for the criterion:

$$\int_V \int_T p'(x,t)q'(x,t)dtdV \geq \int_V \int_T L_i(x,t)dtdV \tag{1}$$

where p' and q' are the instantaneous pressure and heat release rate fluctuations respectively, V is the volume of the resonator, T is the period of the oscillations and L_i is the i^{th} damping process.

Studies of unstable conical flames have been done in unconfined configurations. Noiray *et al.* [4, 5] developed an analytical model that represents the frequency behaviour with respect to the cavity length of the burner for cases with flame and without flame. Furthermore, Ferreira [6] has made a study where the separation between perforations (perfo-

ration ratio) was considered through a factor of impedance given by Maa [7] and found that it influences the results. Although the holes radii and porosity were kept the same, *i.e.* the same number of perforations and the same ratio of perforated area and non-perforated area between plates, the results were different.

Due to climate change problems recent efforts have been made to reduce the amount of green house gases (GHG) emitted to the atmosphere. As a consequence, hydrogen (H_2) has been proposed and promoted to use in current combustion applications, since it is a gas with no carbon derivatives associated to its combustion emissions. H_2 application in gas turbines has been tried and researched [8]. However, its application leads to undesired rise in nitrogen oxides (NOx) emissions.

Lantz *et al.* [9] studied the influence of H_2 addition up to 80% in volume on NOx formation and found that compared to the baseline of natural gas composition, the NOx emissions increase with H_2 addition, reaching 50% increase of NOx emissions when using 80% H_2. Notwithstanding the previous study, ways to reduce NOx emissions with H_2 use have been achieved. Griebel *et al.* [10] found that H_2 extends the lean-blowout limit (LBO) which in turn reduces the firing temperature, leading to lower NOx emissions. Values up to 35% reduction were reached when compared to pure CH_4 flames, even though for $\phi < 0.5$ the difference found in NOx emissions reduction between CH_4 and CH_4+H_2 flames was negligible. Runyon [11] concluded that in practical applications, the addition of H_2 increases the reactivity and thermo-diffusive effects of the mixture, which in turn allow a stable and low NOx operation of gas turbines. Additionally, the same study proposed a power law correlation which predicts a reduction of almost 50% in combustion noise amplitudes by mixing up to 15% H_2 in CH_4.

Other applications of H_2 on jet flame burners have been studied, indicating that CH_4+H_2 blends can be used in burners initially designed for CH_4 [12]. Additionally, simple correlations for blow-out in premixed hydrogen-enriched natural gas (HENG) systems have been deduced, providing an aid in designing new HENG burners or modifying already existing ones [13]. Moreover, H_2 has also been studied in the field of thermoacoustic instabilities [14–16]. Lim *et al.* [14] made a numerical analysis of hydrogen enriched flames and found that it would enhance vibrations at higher frequencies and change the flame shape. Karlis *et al.* [15] made experimental studies on the effects of H_2 enrichment on gas turbine combustors and found that the addition of H_2 up to 10% leads to higher flammability limits, *i.e.* leads to blow-off at lower equivalence ratios, but if its content is further increased random bursts of dynamic pressure and heat release start to appear. Kim *et al.* [16] found that a shift to higher resonance modes were associated with an increase of H_2 in the fuel mixture.

2. Experimental Setup

2.1. Burner and Multiperforated Plates

The experiments done in this thesis are based on a burner geometry where small conical flames are anchored on thin perforated plates. Additionally, the burner has a cavity with variable length and a premixed injection system. A schematic of the burner configuration can be found in figure 1. The fuel and air are injected into the premixing pipe (1). The mixture reaches the burner cavity through twelve orifices equally spaced around the piston head (2), which has 42 mm of diameter. After the mixture exits the orifices, it flows through the variable length cavity (3) with an inner diameter of 43.5 mm and ends at the MPP (4) where the flames are anchored. The burner cavity is varied from 6 cm to 45 cm in the experiments performed for this work. The piston head is flat, which provides a quasi-perfect acoustical reflection boundary and the gap between the piston and cavity diameters is covered by an Teflon O-ring.

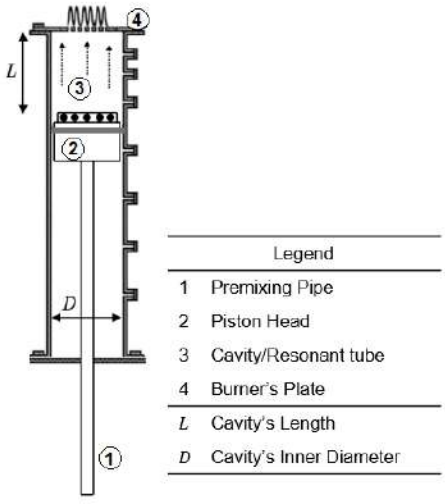

Figure 1: Burner configuration with its components.

Five burner plates (see figure 2) are analysed, these are made from stainless steel and a thickness of 0.5 mm. Each plate has 19 holes of 1.5 mm diameter, all with porosity $\mathcal{P} = 2.3\%$ but different perforation ratios (ψ). The perforation ratio is a parameter given as follows:

$$\psi(\%) = \frac{S_f}{S_a} \approx 90.69(\frac{2r_h}{b})^2 \qquad (2)$$

where S_f, S_a, r_h and b are the cross-sectional area

of perforation, hexagonal area of perforation, hole radius and distance between the centre of the holes respectively. Table 1 summarizes the burner and plate parameters.

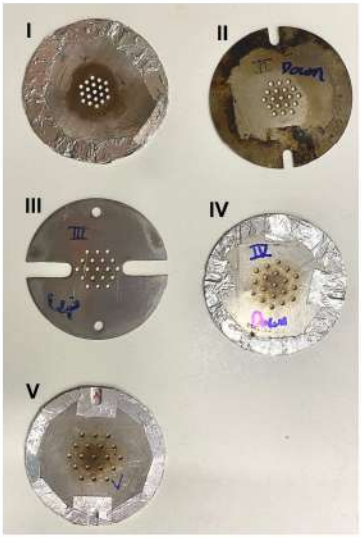

Figure 2: MPPs used in the experiments. Perforation ratio reduces from I to V.

Table 1: Geometrical parameters of the burner and plates.

Parameter	**Value**
Cavity Length (L)	60<L<450 mm
Cavity Internal Diameter (D)	43.5 mm
Plate hole diameter (d_h)	1.5 mm
Number of holes (n_h)	19
Porosity ($\mathcal{P}$)	2.3%
Plate thickness (l)	0.5 mm
Perforation Ratio (ψ)	
Plate I	35.5%
Plate II	26.9%
Plate III	20.5%
Plate IV	13.1%
Plate V	5.7%

2.2. Fuel Blends

The experiments were conducted with the mixture at atmospheric pressure and temperature, with Re from 60 to 275 and $0.5 \leq \phi \leq 1.8$. Re and ϕ are defined as follows:

$$Re = \frac{u\, d_h\, \rho}{\mu} \tag{3}$$

$$\phi = \frac{\mathrm{AFR}_{st}}{\mathrm{AFR}} = \frac{(Q_{air}/Q_{fuel})_{st}}{Q_{air}/Q_{fuel}} \tag{4}$$

where u, ρ and μ are the mean mixture's velocity, mixture's density and mixture's dynamic viscosity respectively. AFR is the fuel-to-air ratio, the subscript st means the stoichiometric value of that property and Q_i is the absolute volumetric flow for the i fluid. Q_{fuel} is defined by the sum of the volumetric flow rates of the fuels used for that experiment. The fuel blends used were 100% C_3H_8, 100% CH_4 and 90% CH_4 + 10% H_2 in volume (v/v).

The flowrate of each gas and air were individually controlled by flowmeters. Alicat Scientific M series mass flow meter of 5 standard litres per minute (SLPM) was used to regulate methane and propane, while another flowmeter of 50 SLPM was used for air and 1 SLPM for hydrogen.

2.3. Equipment and Data Acquisition

Pressure oscillations and frequency of the instabilities were measured using a Bruel Kjr – Type 4189 condenser microphone at a radial distance of 150 mm from the burner centre. A BK 2250 pre-amplifier was used to boost the signal picked from the microphone and the data was acquired by the Data Translation DT9841-VIB-SB acquisition board. The data acquired by the data acquisition board was post-processed and the response of the thermoacoustics was obtained in the frequency domain through a Fast Fourier Transformation (FFT). The digitalization introduced in the Data Translation DT9841-VIB-SB board has an error of 0.3 mV in absolute amplitude, which represents less than 0.1% of its maximum, allowing us to neglect it when going through the procedures [17].

High-speed videos of the flame oscillations were recorded with a Phantom v4.2 camera with a capture rate of 5000 frames per second (fps) at 320×240 pixels resolution and a capture rate of 9009 fps at 256×192 pixels resolution. A full schematic of the experimental setup overview is shown in figure 3.

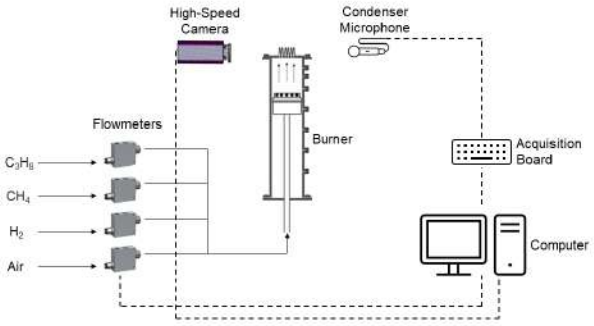

Figure 3: A schematic representation of the experimental setup. Solid lines are where the fuel flows and dashed lines are where data/information flows.

3. Mathematical Model

3.1. Burner Acoustics Model

For the acoustic model of the burner, it is considered that the tube cavity can be modelled as a per-

fect tube with one end closed by a wall and the other by a perforated thin plate. It was also assumed that only the longitudinal acoustic modes are relevant inside the tube, since the cavity length is larger than the its diameter ($L \gg D$). The tube without a perforated plate is considered open ended and its specific acoustic impedance $z = p'/u'$, where p' and u' are the pressure and velocity fluctuation of the flow respectively, would disappear in the exhaust section. With the perforated plate covering the end of the tube, a solution with the effects of the plate's impedance needs to be taken into account. For this, an analysis based on previous studies done by Tijdeman [18] is presented here.

It is possible to show that the shear wave number (s), reduced frequency number (k), square root of the Prandtl number (σ) and specific heats ratio (γ) determine the solution of a propagating wave for tiny sinusoidal amplitudes of a flow inside a rigid tube.

$$s = r\sqrt{\frac{\rho_s \omega}{\mu}} \tag{5}$$

$$k = \frac{\omega r}{c} \tag{6}$$

$$\sigma = \sqrt{\frac{\mu C_P}{\kappa}} \tag{7}$$

$$\gamma = \frac{C_P}{C_V} \tag{8}$$

If we consider the values of σ and γ constant, we end up with only the shear wave number (or Stokes number) and the reduced frequency number to work with. For $k \ll 1$ and $k/s \ll 1$, the solutions of the Low Reduced Frequency are valid [18]. The final solutions for pressure, axial velocity, density and temperature perturbations in the Low Reduced Frequency are:

$$\tilde{p} = A_1 e^{\Gamma\xi} + B_1 e^{-\Gamma\xi} \tag{9}$$

$$\tilde{u} = \frac{i\Gamma}{\gamma}\left[1 - \frac{J_0(i^{3/2}\eta s)}{J_0(i^{3/2}s)}\right]\left(A_1 e^{\Gamma\xi} - B_1 e^{-\Gamma\xi}\right) \tag{10}$$

$$\tilde{\rho} = \left[1 - \frac{\gamma - 1}{\gamma}\left(1 - \frac{J_0(i^{3/2}\sigma\eta s)}{J_0(i^{3/2}\sigma s)}\right)\right] \times \left(A_1 e^{\Gamma\xi} + B_1 e^{-\Gamma\xi}\right) \tag{11}$$

$$\tilde{T} = \frac{\gamma - 1}{\gamma}\left[1 - \frac{J_0(i^{3/2}\sigma\eta s)}{J_0(i^{3/2}\sigma s)}\right]\left(A_1 e^{\Gamma\xi} + B_1 e^{-\Gamma\xi}\right) \tag{12}$$

where η is the radial non-dimensional coordinate ($\eta = r/R$), ξ is the axial non-dimensional coordinate ($\xi = x/L$) and Γ is defined as:

$$\Gamma = \frac{J_0(i^{3/2}s)}{J_2(i^{3/2}s)}\sqrt{\frac{\gamma}{n}} \quad \text{with, } n = \left[1 + \frac{\gamma - 1}{\gamma}\frac{J_2(i^{3/2}\sigma s)}{J_0(i^{3/2}\sigma s)}\right]^{-1} \tag{13}$$

The values of constants A_1 and B_1 are determined by defining additional boundary conditions at both ends of the tube, J_0 and J_2 are the Bessel functions of the first kind for integers 0 and 2 respectively. Equations 11 and 12 can be ignored since the thermal acoustic boundary layer (0.2 mm) is small compared to each hole's diameter (1.5 mm) and therefore the heat transfer from the MPP to the feeding flow is negligible in overcoming the pressure gradient imposed to the holes.

With the equations presented so far, the specific acoustic impedance of the open tube (without the plate) can be treated as:

$$z_{tube} = \rho c \frac{\tilde{p}}{\tilde{u} \cdot \boldsymbol{n_b}} = \rho c \frac{A_1 e^{\Gamma\xi} + B_1 e^{-\Gamma\xi}}{\frac{i\Gamma}{\gamma}\left[1 - \frac{J_0(i^{3/2}\eta s)}{J_0(i^{3/2}s)}\right]\left(A_1 e^{\Gamma\xi} - B_1 e^{-\Gamma\xi}\right)} \tag{14}$$

For the addition of the plate's impedance it is assumed that the burner can be modelled as a large tube and the perforated plate can be modelled as multiple small tubes with a length equal to the plate thickness, leading to a total burner impedance $z_{burner} = z_{tube} + z_{plate}$. The impedance defined by equation 14 has two unknowns in $A1$ and $B1$, meaning that the total burner impedance expression has four unknowns (two for the tube and two for the plate). Therefore, four boundary conditions must be applied to the model (see figure 4). At the piston surface $x = 0$, the axial velocity is zero since it is a closed end; at the boundary between the tube and plate $x = L$, the pressure is continuous between tube and holes inlet; still at $x = L$, there is mass flow conservation; at the plate's exit $x = L + l$, the pressure meets the external conditions.

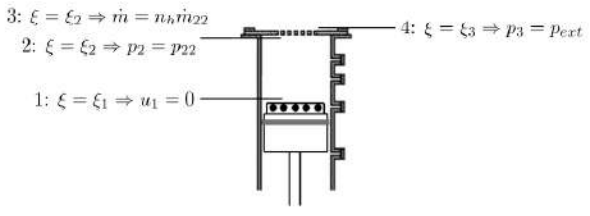

Figure 4: Boundary conditions applied to the burner for the mathematical model.

The only remaining parameter to introduce is the perforation ratio ψ. Following Maa [7], the complete burner impedance is:

$$z_{burner} = z_{tube} + z_{plate} = \frac{\tilde{p}_2}{\tilde{u}_2 \cdot \boldsymbol{n_b}} + \left(\frac{\tilde{p}_3 - \tilde{p}_2}{\tilde{u}_3 \cdot \boldsymbol{n_b}}\right)\frac{1}{\psi} \tag{15}$$

The definition of ψ is given by equation 2 and it relates to the separation between perforations,

opposing to porosity $\mathcal{P}$ which relates to the ratio of perforated and non-perforated area. In this work, the porosity of the different plates is maintained constant at $\mathcal{P} = 2.3\%$.

This mathematical model for the burner acoustics was validated using plate I. Through figure 5 it is possible to observe that the assumption of only longitudinal waves through the tube is capable of modelling the burner acoustics [6].

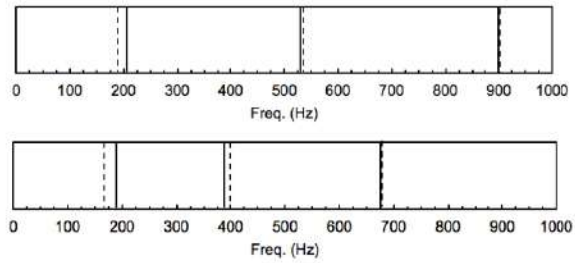

Figure 5: Experimental (solid lines) and mathematical model (dashed lines) results for the resonant modes of the burner with plate I done by Ferreira [6]. Bottom: $L = 57$cm. Top: $L = 42$cm.

3.2. Flame Model

The heat release rate fluctuations generate a pressure fluctuation at the same frequency, meaning that the pressure fluctuation is proportional to the heat release rate fluctuation. It is possible to use the flame surface area as a parameter to compute the heat release since the flame surface is roughly proportional to the heat release rate [5], leading to the following definition for the pressure fluctuation:

$$p' = \frac{\rho_\infty}{4\pi H}\left(\frac{\rho_u}{\rho_b} - 1\right) S_L \left[\frac{\partial A'}{\partial t}\right]_{t-\tau_{ac}} \tag{16}$$

where τ_{ac} is the acoustic propagation delay, corresponding to the time delay that the pressure wave generated at the tip of the flame reaches the burner's exit. ρ_∞ is the volumetric weight of the surrounding air, ρ_u and ρ_b are the unburned and burned gases volumetric weight respectively, H is the distance from the tip of the flame to the burner's exit (which is the flame height H_f), A' is the flame surface area fluctuation and S_L is the laminar flame speed of the mixture.

To evaluate the heat release in an analytical formula, the Flame Transfer Function (FTF) method is used. The FTF is used to characterise the flame response to the imposed velocity oscillations through a transfer function:

$$FTF(\omega) = \frac{q'/\bar{q}}{u'/\bar{u}} = G_\omega e^{i\omega\tau_{cv}} \tag{17}$$

G_ω is the function's gain and τ_{cv} is the convective time delay, which is the time that perturbation from the burner's exit takes to the flame's tip. An experimentally obtained FTF for the burner configuration used in this work was achieved by Leitão [19]. The gain and phase of the FTF are:

$$G_\omega = \left|\frac{0.96}{1 - 1.258i\,(\omega/2999) - (\omega/2999)^2}\right| \tag{18}$$

$$\varphi = \frac{2.33\pi}{1000} f \tag{19}$$

Considering the complex form of the velocity and pressure fluctuations and the definition of impedance, the flame impedance equation becomes:

$$z_{flame} = \frac{\tilde{p}}{\tilde{u}\cdot\boldsymbol{n_f}} = -i\omega\frac{\rho_\infty}{4\pi H}\left(\frac{\rho_u}{\rho_b} - 1\right) S_L G_\omega \frac{\bar{A}}{\bar{u}} e^{i\omega t} \tag{20}$$

3.3. Energy Balance

Recalling the formulation given by Zinn [3] in equation 1 it is possible to interpret the requirement for self-sustained oscillations as the existence of a driving power P_{driv} superior to the dissipative power P_{diss}:

$$|P_{driv} > P_{diss}| \tag{21}$$

The power can be calculated in a surface (S) between the flame and burner and over a period of oscillation T:

$$P = \int_S \frac{1}{T}\int_0^T \Re(p')\Re(u'\cdot\boldsymbol{n}),\, dtdS \tag{22}$$

where $\Re(a)$ is the real part of a. When computing equation 22 as a harmonic perturbation and substituting in equation 21:

$$\frac{S}{2}\,|\Re(z_{flame})|\,|\tilde{u}|^2 > \frac{S}{2}\Re(z_{burner})\,|\tilde{u}|^2 \tag{23}$$

Using the definitions of z_{flame} and z_{burner} given by equations 20 and 15 respectively, it is possible to determine which frequencies can lead to resonance given the working conditions of the burner.

4. Results

4.1. LBO limits and Stability Maps

Results for all plates show a significant higher ϕ for C_3H_8 limits, even spanning rich values ($\phi > 1$) for Re above 200 in plate III, Re above 125 in plate IV and even Re below 100 in plate V. The line shown for each graph in figure 6 represents the LBO limit. The CH_4 fuel allows a significant extension of the LBO limit, leading to a reduction up to around 0.3 in ϕ at $Re = 260$, show in plates IV and V at $Re = 260$. Additionally, although the fraction of H_2 was only 10%, its influence is already noticeable. A relevant extension of the LBO limit is

seen when compared to the pure CH_4 blend, suggestion that with higher H_2 fractions the limits can be further extended and leaner applications may be used without changing the burner's geometry. Even though, plates I and II do not have a very noticeable difference between their limits, the results for other plates show otherwise. A lower ψ leads to a decrease of the limits, even pushing the CH_4 and 10%H_2 blends to richer values in plate V. This is expected since the small flames from each hole have less possibility to sustain each other as they get further apart.

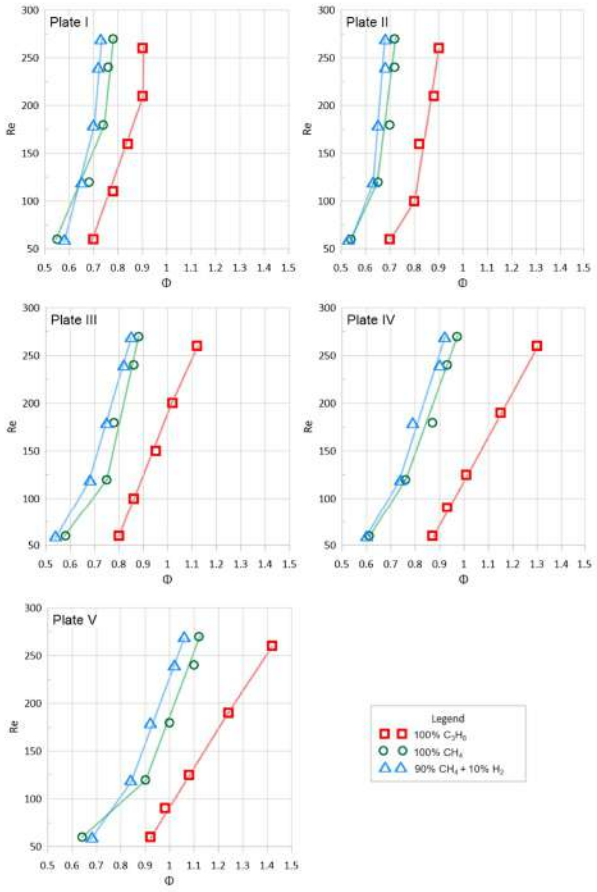

Figure 6: Lean blow-off limits for the different plates and fuels at $L = 12\,\text{cm}$.

C_3H_8 noise regions are larger for all plates when compared to the other fuel blends studied in this work (see figure 7), and in particular, plate V does not manifest a noise region for both 100% CH_4 and 90% CH_4 + 10% H_2. The results for CH_4 show a clear reduction of the noise region when compared to C_3H_8, leading to a wider range of values for which the burner can run with no thermoacoustic instabilities. Yet, similar to the case for propane's plate I map, the margin between the LBO limit and noise region in plate I is very small, not allowing lean working conditions of the burner without generation of noise. Lean conditions with no thermoacoustic instabilities are found in plate I with the addition of H_2. This is due to the combination of a leaner LBO limit and the noise region shifting to richer values. No relevant size difference was found for the noise regions of plates I and II between 100% CH_4 and 90% CH_4 + 10% H_2, but a significant increase exists for plates III and IV. This suggests that an increase use of hydrogen in fuel mixture can lead to even wider undesired noise limits, since a presence of only 10% H_2 in volume has led to such expressive results.

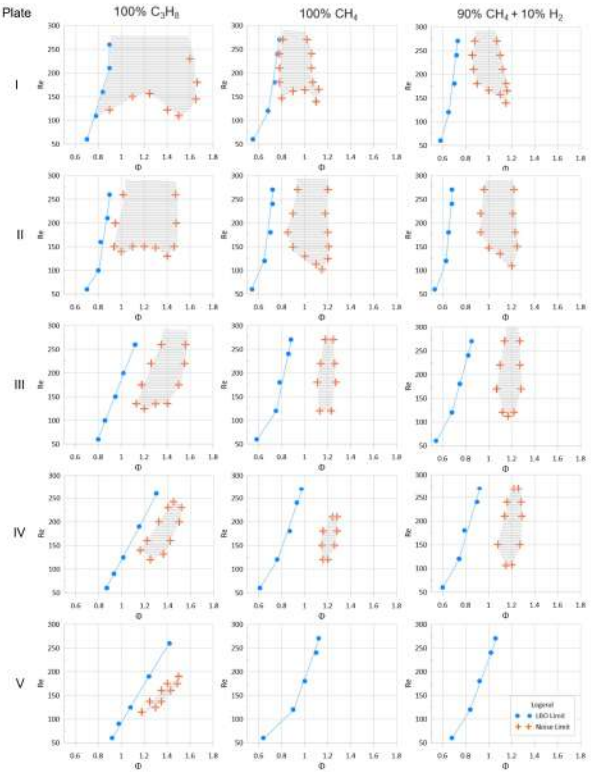

Figure 7: Stability maps for all plates and fuels studied at $L = 12\,\text{cm}$. Shaded sectors represent the thermoacoustically unstable regions.

4.2. Frequency and Sound Pressure Level in Noise Regions

For plate I with both fuel blends (see figure 8 and 9), even though the noise limits shifted to higher ϕ with the addition of H_2 seen from previous results, a slight peak of SPL exist at around $\phi = 1$ for both fixed Re studied of 220 and 180. This is a common factor with results shown by Ferreira [6], as it was also shown that SPL had a slight peak at $\phi = 1$ for plate I but using C_3H_8. At a fixed $\phi = 0.9$, SPL has a tendency to drop at higher Re.

The SPL with respect to ϕ has a different behaviour for plate II when compared to plate I. In-

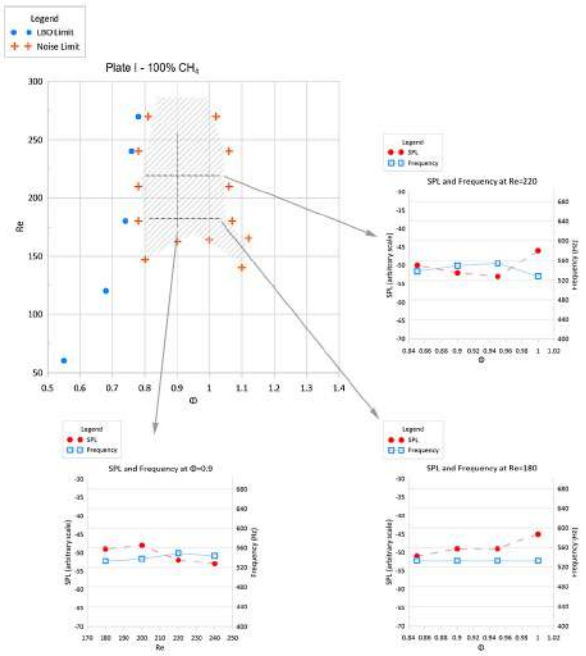

Figure 8: Plate I 100% CH_4 stability map at $L = 12\,\text{cm}$ with frequency and sound pressure level analysis for selected ϕ and Re.

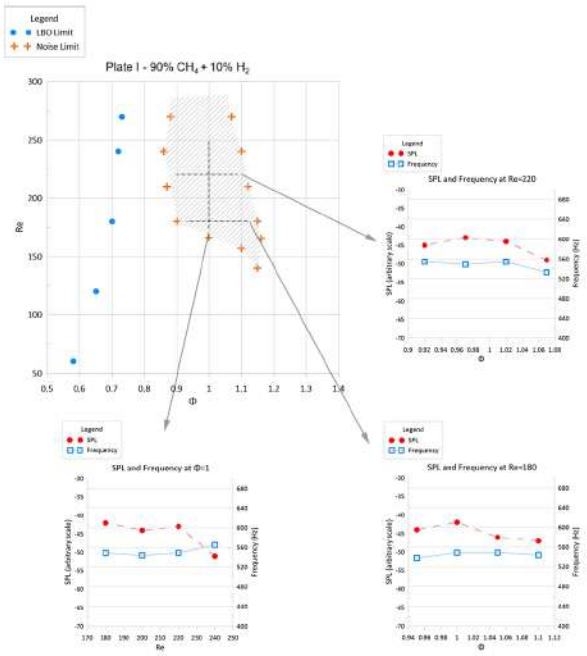

Figure 9: Plate I 90% CH_4 + 10% H_2 stability map at $L = 12\,\text{cm}$ with frequency and sound pressure level analysis for selected ϕ and Re.

stead of a slight peak at $\phi = 1$, SPL continues to rise as ϕ goes higher. More noticeable, frequency has a significant decrease with respect to ϕ for both fuel blends. This drop is found for values of $\phi > 1$. It is a result not found for other plates, demonstrating an uniqueness for plate II. When ϕ is fixed, a disparity between both fuels exists, as 100% CH_4 results in a monotonous behaviour of SPL and frequency while 90% CH_4 + 10% H_2 demonstrates a drop of frequency and rise in SPL for higher Re. Frequency for both fuel blends does not change significantly with respect to ϕ and Re for plates III and IV. The only significant difference is the SPL increase of plate III at higher Re while fixing ϕ at a constant value. The frequencies for the hydrogen enhanced mixtures were slightly higher than the methane counterpart for all plates, being in agreement with results of Kim *et al.* [16] where a shift to higher modes of resonance (higher frequencies) was correlated to a higher fraction of H_2 in the fuel composition, a consequence from the time delay reduction of the flame perturbation.

4.3. Thermoacoustic Instabilities' Flame Shape

A common observation for all results is that the main oscillation mode is in the longitudinal direction as assumed in section 3.1. However, for $Re = 180$, $\phi = 1$ and 100% CH_4 with plate I (figure 10(a)) there are other relevant modes of oscillation. In this case it is possible to observe a transversal mode of oscillation, with the flames separating from each other, meaning that the first assumption made of only longitudinal modes may not always be correct. With the addition of H_2 those transversal modes are not observable, indicating that the presence H_2 can stabilize such interactions. An explanation for the particular case of $Re = 180$, $\phi = 1$ and 100% CH_4 showing transversal modes of oscillation is the interaction between each flame. Since plate I is the plate with the closest holes, the flames here have the highest possibility to interact with each other and therefore, influence each other which happens in a transversal direction. With the addition of H_2 the mixture has a higher flame speed, and therefore reduces its surface area which in turn diminishes the interactions with adjacent flames.

In the results of plate II the most iconic observation is the bubble of flame formation at the tip of the flame, a phenomena also observed in [5, 6]. In figure 10(c), as the flames are going down in their oscillation cycle a quantity of mixture remains at the tip and detaches from the rest of the flame, forming said bubble. This bubble then burns as the flames are already at the lower points. The addition of hydrogen shown in figure 10(d) makes the bubble at the tip disappear. The high flame speed induced by the presence of H_2 leads to a smaller flame area and faster burning speed which does not allow the presence of remaining mixture to be burnt

and detach from the flame base. Another observation is the height and width of the flame at the lower point. In the results for pure CH_4 the flame base is much lower than the H_2 added mixture, suggesting that the presence of H_2 makes the flame base stabler. The width of the flame shows the same behaviour, implying a reduction and less interaction between flames with the addition of H_2.

Recalling the results found in the previous section where there is a slight increase in frequency for the H_2 enhanced blend, results show that by adding H_2 the unstable length of the flame, *i.e.* the portion of the flame that oscillates, is diminished through a combination of lower flame height and higher stable flame base, which can be an explanation for the frequency increase. This phenomena is related to the speed of sound of the mixture with the addition of H_2. As H_2 is added into the mixture, the speed of sound increases and therefore, the acoustic resonance of the burner increases (the burner acts as a Helmholtz resonator). On the other hand the lower flame height induces more gain for the FTF at higher frequencies. With the increase of oscillations at higher frequencies for both the burner and flame, thermoacoustic instabilities with higher frequencies are encouraged.

4.4. Cavity Length Variation and Model

As the cavity length L is increased, frequencies show a jumping behaviour when approaching lengths of 20 cm and above depending on the plate studied (see figures 11 to 13). Despite the complete resonant mode of the burner with flame having differences to the resonant mode of the burner alone represented in the results, the instabilities' frequencies are close to the burner's resonance ones. Both of these phenomena are also found and studied in [4–6], as all show the saw-tooth behaviour of frequency with respect to L.

Observation through the plates indicates that thermoacoustic instabilities are minimized for the interval of L studied as the perforation ratio ψ decreases, specifically the reduction occurs more predominantly at higher L. This also occurs for the results obtained in [6], where the working fuel was 100% C_3H_8 and the plates were the same. In that study, the L span was from 10 to 70 cm and it was found that the instabilities are reduced with the decrease in ψ.

No instabilities were found at fixed $L = 12\,\text{cm}$ for 100% CH_4 and 90% CH_4 + 10% H_2 with plate V previously. However, at $15\,\text{cm} \leq L \leq 21\,\text{cm}$ using the 10% H_2 fuel there are instabilities resonating at around $f = 400\,\text{Hz}$ (see figure 13). In these cavity lengths, the dissipative power is not enough to overcome the driving power (recall equation 23) and therefore noise was sustained.

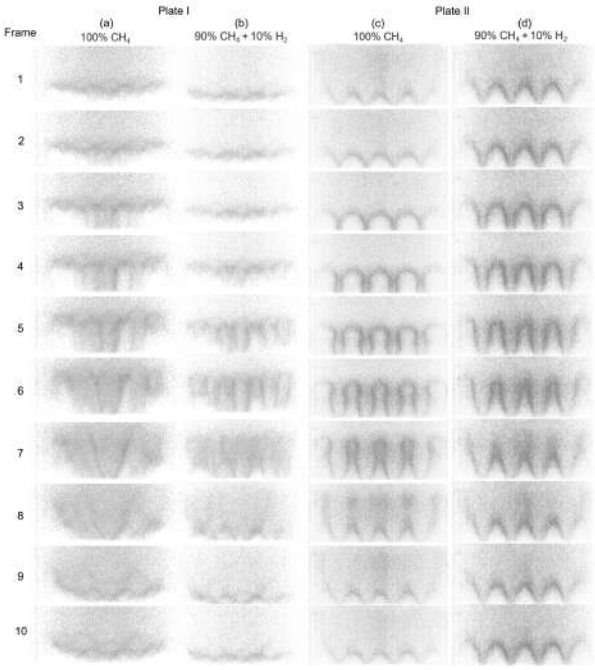

Figure 10: Cycle of flame oscillations at $L = 12\,\text{cm}$ with plates I and II captured by the high-speed camera Phantom V4.2. Time period between each frame is 0.0002s.
(a) Plate I, $Re = 180$, $\phi = 1$, $f = 528\,\text{Hz}$ and 100% CH_4.
(b) Plate I, $Re = 180$, $\phi = 1$, $f = 533\,\text{Hz}$ and 90% CH_4 + 10% H_2.
(c) Plate II, $Re = 220$, $\phi = 1$, $f = 598\,\text{Hz}$ and 100% CH_4.
(d) Plate II, $Re = 220$, $\phi = 1$, $f = 614\,\text{Hz}$ and 90% CH_4 + 10% H_2.

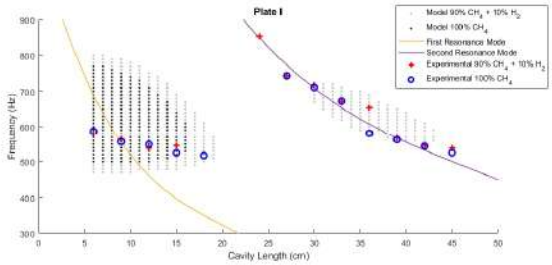

Figure 11: Frequencies with respect to cavity length and model results for plate I. $Re = 220$ and $\phi = 1$.

Fuel wise, the H_2 enhanced mixture does seem be more prone to thermoacoustic instabilities, as the results show the presence of noise for cavity lengths in which the pure CH_4 mixture does not. This is predominant for the frequencies close to the second resonant mode, as the ones related to the first mode appear in the same quantity for both fuels in all

plates besides plate V.

The noise frequencies follow the burner's resonance values only for the ones close to the second mode of resonance. The ones related to the first mode have a more monotonous behaviour with respect to L not following the steeper slope of the burner's resonance mode. This can be explained by the fact that for the burner's acoustic mode in section 3.1 it was assumed that only the longitudinal acoustic modes were relevant. However, transversal modes of oscillation have been found in results from flame shape analysis meaning that the first assumption made is incorrect.

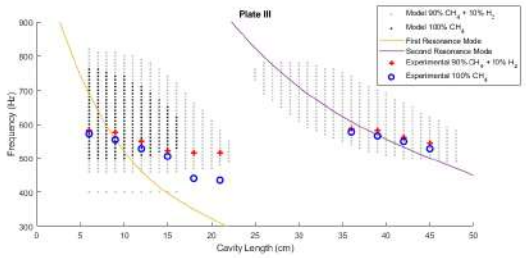

Figure 12: Frequencies with respect to cavity length and model results for plate III. $Re = 180$ and $\phi = 1.19$.

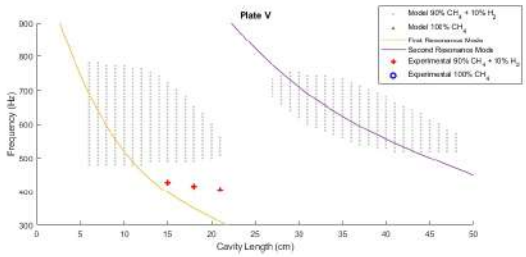

Figure 13: Frequencies with respect to cavity length and model results for plate V. $Re = 160$ and $\phi = 1.2$.

Lastly, the model's results show that it does not predict correctly at which length and frequencies instabilities may occur. Although for plates I and II the region where the model predicts instabilities are concurrent with the experimental data for the frequencies related to the first mode of resonance, the instabilities related to the second mode are not well predicted. This problem is further enhanced for the remaining plates, where in plate IV and V the majority of the results are shown outside the model's areas.

5. Conclusions

The objective of this work was to study the onset of thermoacoustic instabilities for different geometrical configurations of the burner and different fuel blends in order to evaluate the suitability of current burners for the use of H_2. With that in mind, experiments in a burner with the capability to change its cavity length were done in addition to usage of different fuel blends and stabilizing plates with distinct ψ. A mathematical model to predict the instabilities was also evaluated. The relevant findings are:

1. Hydrogen addition in the mixture allowed leaner operation modes. However, as the plates' holes were distanced farther apart, flames could only be sustained for richer mixtures.

2. Thermoacoustic instabilities are more prone to appear for propane mixtures when compared to the methane and hydrogen ones. Hydrogen seems to increase the probability of thermoacoustic instabilities when added to methane.

3. It was found that the higher flame speed induced by hydrogen leads to a stabler flame base and lower flame height, this in turn conveys a shorter length for which the flame oscillates leading to a frequency increase, analogous to the reduction of clamped beam's length.

4. The modes of oscillation that dominate thermoacoustic instabilities for this burner are not only in the longitudinal direction, but also in a transversal one. High-speed camera results show that sideways oscillations of the flame are sometimes non-negligible.

5. Sometimes unburned mixture detaches from the flame tip when it is going down in the oscillation cycle, then flame bubbles are formed which burn detached from the rest of the flame.

6. Frequencies of the oscillations were closer to the resonance of the burner alone for higher cavity lengths. This was explained due to the fact that at higher cavity lengths the approximation of only longitudinal acoustic modes was valid, but at lower lengths such assumption cannot be made as transversal modes are also relevant.

7. Although the mathematical model predicted more instabilities for the hydrogen added mixture and less instabilities as ψ decreased, its results were often far off from the experimental counterpart, showing a weak performance.

References

[1] L. Rayleigh. The explanation of certain acoustical phenomena. *Nature*, 18(455):319–321, 1878. doi: 10.1038/018319a0.

[2] A. A. Putnam and W. R. Dennis. Organ-pipe oscillations in a flame-filled tube. *Symposium*

(International) on Combustion, 4(1):566–575, 1953. ISSN 0082-0784. doi: https://doi.org/10.1016/S0082-0784(53)80078-0. Fourth Symposium (International) on Combustion.

[3] B. T. Zinn. Pulse combustion: recent applications and research issues. *Symposium (International) on Combustion*, 24(1):1297–1305, 1992. ISSN 0082-0784. doi: https://doi.org/10.1016/S0082-0784(06)80151-7. Twenty-Fourth Symposium on Combustion.

[4] N. Noiray, D. Durox, T. Schuller, and S. Candel. Self-induced instabilities of premixed flames in a multiple injection configuration. *Combustion and Flame*, 145(3):435–446, 2006. ISSN 0010-2180. doi: https://doi.org/10.1016/j.combustflame.2006.01.006.

[5] N. Noiray, D. Durox, T. Schuller, and S. Candel. Passive control of combustion instabilities involving premixed flames anchored on perforated plates. *Proceedings of the Combustion Institute*, 31(1):1283–1290, 2007. ISSN 1540-7489. doi: https://doi.org/10.1016/j.proci.2006.07.096.

[6] M. Ferreira. Thermoacoustic self-sustained instabilities of conical flames in multi-perforated plate burners. Master's thesis, Instituto Superior Técnico, July 2017.

[7] D.-Y. Maa. Potential of microperforated panel absorber. *The Journal of the Acoustical Society of America*, 104(5):2861–2866, 1998. doi: 10.1121/1.423870.

[8] P. Chiesa, G. Lozza, and L. Mazzocchi. Using Hydrogen as Gas Turbine Fuel . *Journal of Engineering for Gas Turbines and Power*, 127 (1):73–80, 02 2005. ISSN 0742-4795. doi: 10.1115/1.1787513.

[9] A. Lantz, R. Collin, M. Aldén, A. Lindholm, J. Larfeldt, and D. Lörstad. Investigation of Hydrogen Enriched Natural Gas Flames in a SGT-700/800 Burner Using OH PLIF and Chemiluminescence Imaging. *Journal of Engineering for Gas Turbines and Power*, 137 (3):031505, Mar. 2015. ISSN 0742-4795, 1528-8919. doi: 10.1115/1.4028462.

[10] P. Griebel, E. Boschek, and P. Jansohn. Lean Blowout Limits and NO Emissions of Turbulent, Lean Premixed, Hydrogen-Enriched Methane/Air Flames at High Pressure. *Journal of Engineering for Gas Turbines and Power-transactions of The Asme - J ENG GAS TURB POWER-T ASME*, 129, 04 2007. doi: 10.1115/1.2436568.

[11] J. Runyon. *Gas Turbine Fuel Flexibility: Pressurized Swirl Flame Stability, Thermoacoustics, and Emissions*. PhD thesis, University of Cardiff, May 2017.

[12] A. Palacios and D. Bradley. Conversion of natural gas jet flame burners to hydrogen. *International Journal of Hydrogen Energy*, 46(33): 17051–17059, May 2021. ISSN 03603199. doi: 10.1016/j.ijhydene.2021.02.144.

[13] D. R. Jones and C. W. Dunnill. On the initiation of blow-out from cooktop burner jets: A simplified energy-based description for the onset of laminar flame extinction in premixed hydrogen-enriched natural gas (heng) systems. *Fuel*, 294:120527, June 2021. ISSN 00162361. doi: 10.1016/j.fuel.2021.120527.

[14] Z. Lim, J. Li, and A. S. Morgans. The effect of hydrogen enrichment on the forced response of CH4/H2/Air laminar flames. *International Journal of Hydrogen Energy*, 46(46):23943–23953, 2021. ISSN 0360-3199. doi: https://doi.org/10.1016/j.ijhydene.2021.04.171.

[15] E. Karlis, Y. Liu, Y. Hardalupas, and A. M. Taylor. H2 enrichment of CH4 blends in lean premixed gas turbine combustion: An experimental study on effects on flame shape and thermoacoustic oscillation dynamics. *Fuel*, 254:115524, Oct. 2019. ISSN 00162361. doi: 10.1016/j.fuel.2019.05.107.

[16] D. Kim, S. Joo, and Y. Yoon. Effects of fuel line acoustics on the self-excited combustion instability mode transition with hydrogen-enriched laboratory-scale partially premixed combustor. *International Journal of Hydrogen Energy*, 45(38):19956–19964, 2020. ISSN 0360-3199. doi: https://doi.org/10.1016/j.ijhydene.2020.05.074.

[17] E. C. Fernandes. *The Onset of Combustion-Driven Acoustic Oscillation*. PhD thesis, Instituto Superior Técnico, 1998.

[18] H. Tijdeman. On the propagation of sound waves in cylindrical tubes. *Journal of Sound and Vibration*, 39(1):1–33, 1975. ISSN 0022-460X. doi: https://doi.org/10.1016/S0022-460X(75)80206-9.

[19] I. D. V. Leitão. Experimental and analytical flame transfer functions of multi-perforated plate burners. Master's thesis, Instituto Superior Técnico, September 2009.